Ecological Informatics 96 (2026) 103854

Contents lists available at ScienceDirect

Ecological Informatics

journal homepage: www.elsevier.com/locate/ecolinf

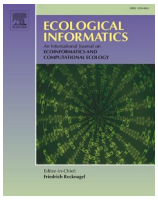

InsectMorphoAI: A deep learning framework for automated insect morphometrics and biomass estimation with taxon-specific volumetric validation

Hossein Shirali [a,*], Aleida Ascenzi [b,c], Lorenz Wührl [a], Nils Beyer [a], Noemi Di Lorenzo [c,d], Emanuele Vaccarella [e], Nathalie Klug [a], Rudolf Meier [f,g], Pierfilippo Cerretti [b,c], Christian Pylatiuk [a]

[a] Institute for Automation and Applied Informatics (IAI), Karlsruhe Institute of Technology (KIT), 76149 Karlsruhe, Germany
[b] Department of Biology and Biotechnologies "Charles Darwin", Sapienza University of Rome, 00185 Rome, Italy
[c] Museum of Zoology (MZUR), Sapienza University of Rome, 00162 Rome, Italy
[d] Department of Life Sciences, University of Siena, 53100 Siena, Italy
[e] Department of Environmental Biology, Sapienza University of Rome, 00185 Rome, Italy
[f] Center for Integrative Biodiversity Discovery, Museum für Naturkunde, Leibniz Institute for Evolution and Biodiversity Science, Invalidenstraße 43, 10115 Berlin, Germany
[g] Institute of Biology, Humboldt University, 10115 Berlin, Germany

ARTICLE INFO

Keywords:
Automated morphometrics
Deep learning
Biodiversity monitoring
Insect biomass
Oriented bounding boxes
Instance segmentation

ABSTRACT

Accurate measurement of insect morphometric traits is essential for functional ecology and biodiversity monitoring. Yet traditional manual methods are labor-intensive, invasive, destructive, and difficult to scale within high-throughput biodiversity pipelines. InsectMorphoAI is an open-source, dual-module framework that automates specimen-level trait extraction from standard 2D images using deep learning. A hardware-agnostic Oriented Bounding Box (OBB) module provides rotation-invariant linear length estimation across diverse insect taxa, achieving a mean absolute error of 0.211 mm (≈2.3% of mean specimen length) in an independent validation dataset of bristle flies (Diptera: Tachinidae). A complementary instance segmentation module enables high-precision, taxon-specific trait extraction by delineating the head, thorax, and abdomen to derive curvilinear lengths and approximate 3D body volume using stacked frustums. Implemented and validated here using bristle flies as a proof-of-concept system, segmentation-derived volume explained more variation in body-only biomass than linear length within the validation dataset ($R^2 = 0.823$ for body-only dry weight and $R^2 = 0.880$ for wet weight after leg removal, compared to $R^2 = 0.610$–0.627 for length-based estimates). As a non-destructive approach, the framework preserves specimens for downstream molecular analyses such as DNA barcoding. The modular architecture provides a practical pathway for extending high-precision volumetric estimation through the development of taxon-specific models. Distributed via Docker with a graphical interface and command-line tool, InsectMorphoAI enables reproducible morphometric data acquisition for applications in functional trait ecology, biomass monitoring, and conservation assessments.

1. Introduction

Accurate measurement of insect traits, such as length, volume, and biomass, is fundamental to understanding ecosystem health, functional trait ecology, energy flow through food webs (Cardinale et al., 2012; Loreau et al., 2001), and population responses to environmental shifts (Lister and Garcia, 2018). These morphometric data underpin several ecological sub-disciplines. In functional trait ecology, body size links to dispersal ability and metabolic rate (Bosch and Vicens, 2002). In pollination biology, body-size-related traits can contribute to plant–pollinator trait matching, pollen transport capacity, activity patterns, and foraging range, although pollination efficiency itself depends on multiple interacting morphological, behavioral, phenological, and ecological factors (Bartomeus et al., 2016; Greenleaf et al., 2007;

* Corresponding author.
E-mail address: hossein.shirali@kit.edu (H. Shirali).

https://doi.org/10.1016/j.ecoinf.2026.103854
Received 16 March 2026; Received in revised form 21 May 2026; Accepted 21 May 2026
Available online 25 May 2026

Ramalho et al., 1998; Streinzer et al., 2016). In pest management and behavioral ecology, precise individual-level measurements are essential for assessing pest dynamics and parasitoid–host interactions (LaBarbera, 1989; Maurey et al., 2025). However, the well-documented global decline in insect populations (Hallmann et al., 2017; Sánchez-Bayo and Wyckhuys, 2019) has highlighted a critical data bottleneck: we currently lack scalable morphometric tools to rapidly quantify these community changes. This bottleneck is particularly evident when processing the massive sample volumes generated by standardized continuous collection methods, such as Malaise traps (Karlsson et al., 2020), which often yield thousands of specimens representing hyperdiverse and taxonomically poorly understood groups (Hartop et al., 2022).

Traditional morphometric methodologies, which typically involve direct weighing after oven-drying or manual measurement under a microscope, are precise but inherently invasive, destructive, labor-intensive, and subject to inter-observer variability inherent to manual morphometric protocols (Rogers et al., 1977; Sample et al., 1993). Crucially, destructive methods preclude subsequent molecular analyses such as DNA barcoding, which are increasingly central to modern "reverse workflow" biodiversity assessments in which specimens are barcoded first and morphologically analyzed later (Hartop et al., 2024; Srivathsan et al., 2021; Yeo et al., 2021). The broader field is rapidly converging toward integrated pipelines that combine robotics, high-resolution imaging, high-throughput sequencing, and machine learning to address large-scale insect analysis at scale (Meier et al., 2024; Wägele et al., 2022), encompassing automated specimen handling (Wührl et al., 2022), size-sorting (Ascenzi et al., 2025), high-resolution digitization (Hereld et al., 2017; Klug et al., 2024), and AI-driven taxonomic classification (Caruso et al., 2026; Knyshov et al., 2021; Shirali et al., 2024; Van Dam and Štarhová Serbina, 2025). Within this vision, automated insect morphometrics presents unique computational challenges: the complex 3D articulations of insect bodies create severe occlusions in 2D images, undermining conventional contour-based measurement approaches and motivating the use of deep learning for robust body-part delineation (Shirali et al., 2026c).

Several pioneering systems have attempted to address these challenges, but notable methodological gaps remain. For example, tools that rely on 2D geometric image features as a biomass proxy, such as BIODISCOVER (Ärje et al., 2020), are often limited by inconsistent relationships between features and weight across morphologically diverse groups. Conversely, systems like DiversityScanner (Wührl et al., 2022) successfully approximate 3D volumes but require manual adjustments for complex morphologies and rely on robotic hardware, restricting their deployment to well-funded, specialized facilities. Other deep learning approaches, such as those by Schneider et al. (2022), focus on aggregate biomass estimation across bulk samples rather than on extracting precise morphometric measurements from individual specimens. Consequently, the field lacks a hardware-agnostic, non-destructive computational framework capable of extracting specimen-level volumetric and biomass data in a form accessible to standard entomological workflows. A central but often implicit limitation of existing approaches is a trade-off between generalizability and morphometric precision: methods applicable across taxonomically diverse insect assemblages typically rely on simplified geometric proxies, whereas approaches capable of extracting biologically meaningful traits at high precision require taxon-specific modeling and validation.

To address this limitation, we introduce InsectMorphoAI, an open-source dual-module deep learning framework, designed to reconcile generalizability and morphometric precision within a unified pipeline. Rather than relying on a single universal model, the framework explicitly separates a broadly applicable length estimation module from a taxon-specific segmentation-based module for high-precision trait extraction. Both insect length and volume are established non-destructive proxies for biomass, based on well-known allometric relationships (Ganihar, 1997; Rogers et al., 1977; Sample et al., 1993; Smock, 1980). The first module provides rapid, orientation-aware linear length estimation using an Oriented Bounding Box (OBB) model, trained across multiple insect orders. The second module provides highly granular trait extraction via instance segmentation, delineating specific body parts to extract curvilinear splines and geometrically approximate 3D volume via stacked frustums, which we then correlate with empirical body-only dry weights to validate biomass predictions. Because high-precision segmentation depends on taxon-specific morphology, this module is implemented and validated in a taxon-specific context using a hyperdiverse and abundant family of true flies (Diptera: Tachinidae) as a proof-of-concept system. This choice reflects a deliberate design strategy, allowing evaluation of geometry-based volume reconstruction under controlled morphological conditions. Given that rank-abundance distributions in insect communities are typically dominated by a limited number of families (Srivathsan et al., 2023), a possible future scaling strategy is to develop and validate separate segmentation models for the most frequent families.

By integrating a broadly applicable OBB-based length-estimation component with a taxon-specific segmentation component within a single framework, InsectMorphoAI provides a scalable and non-destructive approach to specimen-level morphometrics.

2. Materials and methods

2.1. Computational framework and implementation

To operationalize the two proposed deep learning modules as a reproducible, accessible tool, we implemented them within a unified computational framework (InsectMorphoAI), written in Python 3.11, utilizing PyTorch as the primary deep learning framework and OpenCV for morphological post-processing. To ensure cross-platform reproducibility and eliminate complex dependency management, the software is containerized and deployed via Docker, meaning that the application and all required software dependencies are bundled into a standardized environment that can be run consistently across operating systems. For users who prefer not to use Docker, the repository also provides instructions for manual installation in a native Python environment. The user interacts with the system through a web-based Graphical User Interface (GUI) built with the Streamlit framework (Streamlit Inc., n.d.).

To accommodate high-throughput requirements, the software supports both single-image analysis and automated batch processing of entire directories. Furthermore, the architecture processes one specimen per image and exports all measurements into a consolidated, analysis-ready CSV file. For practical use, inference can be performed on standard CPU-based computers, although the runtime depends on image resolution, batch size, and the selected analysis module. GPU acceleration is not required for running the software, but is recommended for large batches, especially for the segmentation-based detailed analysis module. Training or fine-tuning additional models is more computationally demanding and is best performed on CUDA-compatible GPUs.

A prerequisite for accurate absolute measurements is spatial calibration, which applies uniformly to both analysis modules. InsectMorphoAI converts pixel-based predictions into physical units (millimeters) using a user-defined scaling factor $\hat{k}$. The parameter $\hat{k}$ is calculated via a reference object of known dimensions (e.g., a micrometer slide) imaged under the same optical conditions, formulated as (Eq. 2.1):

$$\hat{k} = \frac{\text{Object Size in mm}}{\text{Object Size in px}} \tag{2.1}$$

To correct for potential pixel-resolution anisotropy, which can arise in camera and lens systems where horizontal and vertical pixel densities differ, the calibration factor should be computed by imaging the reference object in both orientations and averaging the resulting values. The predefined Entomoscope profiles (Wührl et al., 2024) bundled with InsectMorphoAI already incorporate this correction. The GUI (Fig. 1) includes a predefined list of camera and telecentric lens profiles

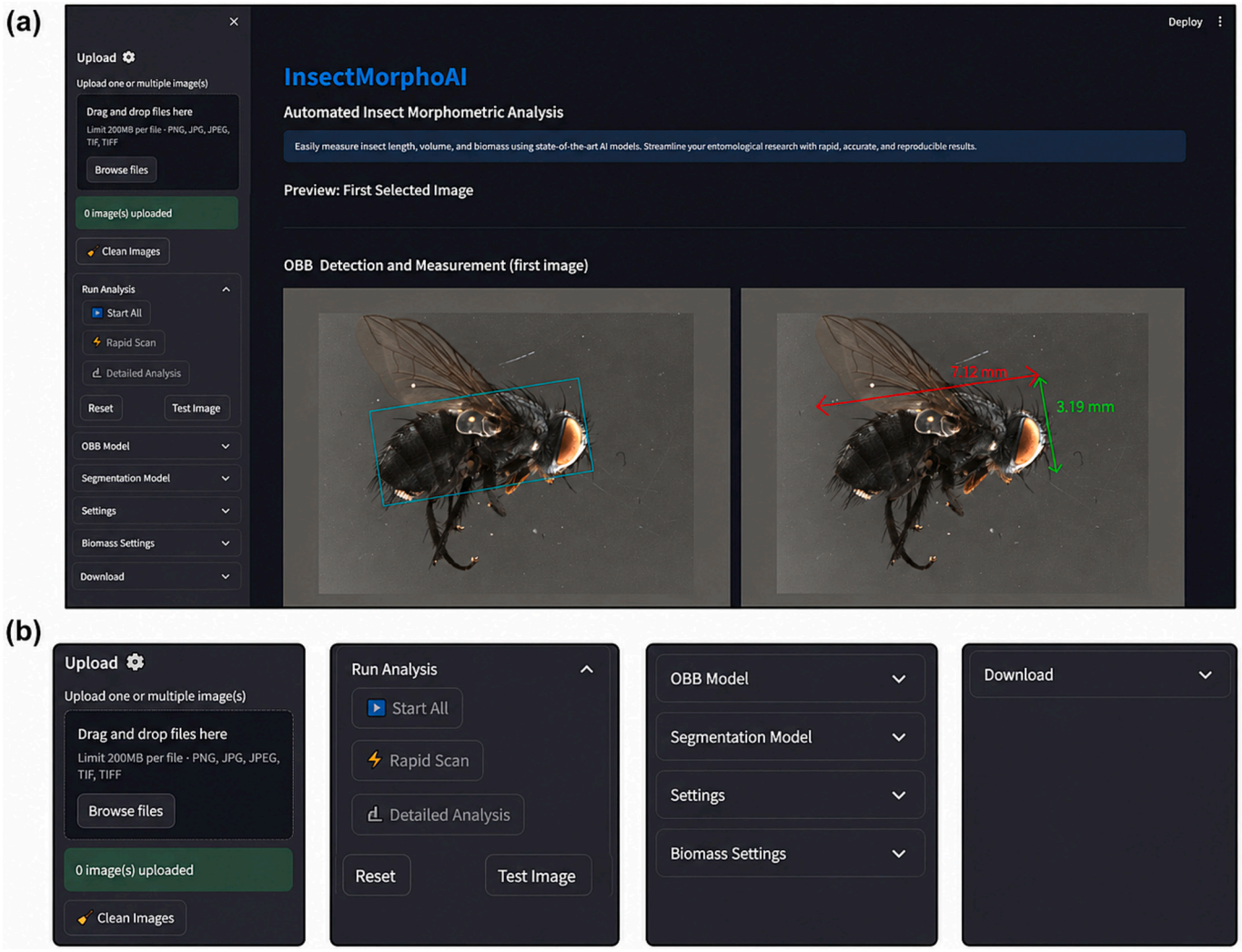

Fig. 1. Overview of the InsectMorphoAI graphical user interface (GUI). **(a)** Full GUI layout, illustrated with the OBB-based rapid length-estimation module. **(b)** Enlarged sidebar components showing image upload, analysis controls, model/settings selection, and download/export options. The segmentation-based detailed analysis module is available through the same GUI and is shown in Fig. 3.

(calibrated for the Entomoscope system) and provides a "Custom Setup" configuration that allows users to input scaling factors for any standard stereomicroscope or camera setup. For non-Entomoscope setups, calibration should be performed separately for each optical configuration using a reference object imaged under the same conditions as the specimens; calibration factors should not be transferred between setups or sessions unless the two configurations have been independently verified to produce equivalent scaling values. The software is released under the MIT License and is available on GitLab (Shirali et al., 2026b), together with all associated datasets on Zenodo (Shirali and Ascenzi, 2026). The analytical core of the framework consists of two independent modules: a generalized length estimation module based on OBB, described in Section 2.3, and a taxon-specific segmentation-based volumetric module, described in Section 2.4.

2.2. Image acquisition and dataset preparation

To train and validate the computational modules, high-resolution images of ethanol-preserved insects, capturing diverse views and orientations, were acquired using the Entomoscope setup (Wührl et al., 2024) and focus-stacked using Helicon Focus (Helicon Soft Ltd., 2025). Because specimens varied in body size, images were acquired using different Entomoscope camera–lens configurations; therefore, morphometric scaling was standardized using setup-specific pixel-to-millimeter calibration factors rather than a single conventional magnification value. To prevent data leakage, both datasets were partitioned by distinct specimen IDs: the segmentation dataset using a 70:15:15 (train:validation:test) split, and the OBB dataset using an 85:15 (train:validation) split, with OBB accuracy evaluated externally against manual photomicroscopy measurements. The present datasets, therefore, represent standardized single-specimen imaging workflows rather than unconstrained bulk-sample imaging scenarios. Images were acquired under controlled Entomoscope lighting and background conditions, and the current models should not be assumed to generalize to field-taken images, cluttered backgrounds, or uncontrolled illumination without additional validation or fine-tuning. To address severe occlusions caused by insect appendages in 2D, we implemented a two-stage annotation strategy.

2.2.1. Initial baseline for general length

For the generalized OBB dataset, 815 images spanning multiple insect orders, including Diptera, Hymenoptera, and Coleoptera, were annotated, representing 804 unique specimens. Bounding boxes were drawn to encapsulate the main body (head, thorax, abdomen) while deliberately excluding non-essential appendages (wings, legs, antennae) to isolate the core elements critical for length measurement. A 10%

spatial padding was automatically applied to images where specimens bordered the image edge to ensure robust bounding box placement.

2.2.2. Refined segmentation strategy

For the taxon-specific segmentation module, we established a high-quality dataset of 1320 images using bristle flies (Diptera: Tachinidae) as a model taxon, representing 702 unique specimens across 105 species. Most specimens contribute one or two images corresponding to different orientations, ensuring that biological variability across individuals drives model generalization. Tachinidae was selected because it provides a useful proof-of-concept taxon for segmentation-based volumetric reconstruction: specimens were available in sufficient numbers, the family has a broadly cylindrical body plan suitable for testing the stacked-frustum approximation, and it still includes substantial variation in body size, posture, and external morphology. Moreover, Tachinidae is among the largest families of Diptera, with approximately 9000 described species (O'Hara and Henderson, 2022) and substantially higher estimated true diversity, making it a biologically meaningful test system rather than an idiosyncratic model group (Stireman III et al., 2021). Thus, Tachinidae represents an intermediate-complexity test case: morphologically tractable enough for geometric validation, but diverse enough to evaluate whether the pipeline can handle realistic variation within a major dipteran group. We first annotated 820 images using Grounding DINO (Liu et al., 2023) and the Segment Anything Model (SAM) (Kirillov et al., 2023). We then utilized this initial model to generate pseudo-labels for an additional 500 images. An expert annotator manually refined these pseudo-labels using LabelMe (Wada, 2018), explicitly inferring and correcting the outlines of core body parts (head, thorax, abdomen) that were partially obscured by wings or legs. This iterative pseudo-label refinement significantly improved the model's robustness against complex poses. Complete specimen details and image lists are provided in Supplementary Data S1 (OBB dataset) and Data S2 (segmentation dataset).

2.3. Module 1: General length estimation via oriented bounding boxes (OBB)

The "Rapid Scan" module is designed for rotation-invariant linear length estimation across morphologically diverse samples. We utilized the YOLOv8-obb architecture (Jocher et al., 2023), which predicts rotated bounding boxes that tightly align with the specimen's longitudinal axis.

We performed transfer learning by fine-tuning models pre-trained on the DOTA (Dataset for Object Detection in Aerial Images) dataset (Xia et al., 2018) on 815 annotated images. Following a systematic evaluation of five architectural variants (nano through extra-large), the YOLOv8m-obb (medium) variant was selected for providing the optimal trade-off between accuracy and computational efficiency, achieving a best validation mAP@0.5 of 0.995 and mAP@0.5–0.95 of 0.846 during training. The training convergence for the selected model is provided in Fig. A1. All models were trained on the HAICORE HPC cluster at the Karlsruhe Institute of Technology using NVIDIA A100 GPUs. The model was trained for 200 epochs using the AdamW optimizer (learning rate = 0.01, batch size = 16) with extensive data augmentations (random rotations, scaling, flipping, mosaic, erasing) to ensure robust orientation generalization. During inference, the linear length is computed by extracting the longest pixel dimension of the predicted OBB and multiplying it by the scaling factor (Fig. 2). Although the OBB also yields a width estimate from the minor axis of the bounding box, this value is less reliable than length due to variability in specimen poses and potential occlusions, and was therefore not assessed as a primary output in this study. Representative cross-order predictions are illustrated qualitatively in Fig. A3, confirming visually consistent OBB placement across Diptera, Hymenoptera, and Coleoptera.

2.4. Module 2: High-precision segmentation and volumetric approximation

The "Detailed Analysis" module provides granular morphometric extraction. Recognizing that precise volumetric reconstruction depends on taxon-specific morphology, we engineered this module as an extensible framework, validated here using the Tachinidae dataset.

2.4.1. Instance segmentation

Model selection was based on both segmentation accuracy and suitability for integration into a deployable morphometric pipeline. On the initial 820-image dataset, YOLOv8-seg (nano variant) outperformed Mask R-CNN (He et al., 2017) (ResNet-50-FPN backbone) in segmentation accuracy (mAP@0.5: 0.944 vs. 0.922), confirming YOLOv8-seg as the preferred architecture. A systematic evaluation of all five YOLOv8-seg size variants on this dataset further showed that the medium variant (YOLOv8m-seg) offered the best accuracy-efficiency balance, achieving mAP@0.5–0.95 of 0.734 compared to 0.686 for the nano variant (Table A1). To produce the final model on the refined dataset, we compared two training strategies: fine-tuning from the model already trained on the initial dataset, versus training directly on the full dataset from COCO-pretrained weights. Fine-tuning outperformed direct training, and the resulting production model achieved a segmentation mAP@0.5 of 0.995 on the held-out test set. Training utilized the Adam optimizer for 100 epochs (learning rate = 0.01, weight decay = 0.0005). The final model produces precise, pixel-level masks that independently classify the head, thorax, and abdomen. Training performance of the final YOLOv8m-seg model is provided in Fig. A2.

2.4.2. Curvilinear length extraction via spline interpolation

To extract the true curvilinear body length, accounting for natural curvature in preserved specimens, the module calculates the center of gravity (CoG) for each predicted segmentation mask (head, thorax, abdomen). A parametric natural cubic spline, enforcing C^2 continuity at the knot points and zero second-derivative boundary conditions at the

Fig. 2. Workflow of the OBB-based rapid length-estimation module. The input image shows an ethanol-preserved insect imaged individually with the Entomoscope system. Absolute measurements were obtained using setup-specific pixel-to-millimeter calibration factors. Left: input image. Center: predicted oriented bounding box (OBB). Right: final output showing the derived linear length (red) and width (green) measurements. A 10% padded border was used during training to improve OBB placement for specimens near the image edge. (For interpretation of the references to colour in this figure legend, the reader is referred to the web version of this article.)

endpoints, is fitted through these three CoG coordinates to model the body's central axis. The spline curve is then linearly extended to intersect the anterior boundary of the head mask and the posterior boundary of the abdomen mask. Total curvilinear length is derived by summing the arc lengths of these discrete spline segments.

2.4.3. 3D volume approximation via stacked frustums

To approximate 3D volume from 2D segmentation masks, the module mathematically models the insect body as a series of stacked geometric frustums (truncated cones) (Wührl et al., 2022). Orthogonal lines are generated at equidistant intervals along the previously computed curvilinear central axis. The local slope is computed at each sampled point, and the orthogonal line (defined as the negative reciprocal) is extended until it intersects the outer boundary of the combined segmentation mask. The distance between the two boundary intersection points provides the diameter (d_i) of the circular cross-section at that point. The geometric parameterization of the frustum model is illustrated in Fig. A4.

The volume of each discrete frustum segment (V_i^{px}) between adjacent orthogonal cross-sections is calculated as:

$$V_i^{px} = \frac{h_i}{12}\pi\left(d_i^2 + d_i d_{i+1} + d_{i+1}^2\right), \quad i = 1, 2, \ldots, N_{midline} - 1 \tag{2.2}$$

Where h_i is the interval distance along the centerline, and d_i and d_{i+1} are the respective cross-sectional diameters measured in pixels. The total specimen volume is approximated by summing the piecewise volumes:

$$V_{total}^{px} = \sum_{i=1}^{N_{midline}-1} V_i^{px} \tag{2.3}$$

The final output is converted from cubic pixels to cubic millimeters by applying the cubic spatial calibration factor ($\widehat{k^3}$). It is important to note that this reconstruction is a geometric approximation rather than a true 3D reconstruction: the *Z*-axis body thickness is not measured directly from the 2D image, but is inferred by assuming that each orthogonal 2D body width corresponds to the diameter of a circular cross-section. This assumption is biologically suitable for the relatively cylindrical body plan of Tachinidae, as validated here, but may introduce systematic bias when applied to taxa with flattened, laterally compressed, strongly irregular, or appendage-dominated morphologies. The method also assumes that specimens are imaged in a standardized view in which the visible body outline provides a meaningful approximation of body width along the centerline; severe contortion, out-of-plane curvature, lateral rolling, or non-standard viewing angles may therefore degrade volume and biomass estimates. The complete segmentation-based workflow, from raw input through body-part masks, centerline extraction, and volumetric reconstruction, is illustrated in Fig. 3.

2.5. Validation protocol and ground truth acquisition

To evaluate the accuracy of the automated predictions, a validation dataset of 100 tachinid specimens representing 23 species (mean length: 9.36 mm; mean body-only dry weight (BODW): 6.1 mg) was established. Prediction accuracy was quantified using the Pearson correlation coefficient (R), the coefficient of determination (R^2), the mean absolute error (MAE), and the root mean square error (RMSE). All reported R values include 95% confidence intervals computed via Fisher's *Z*-transformation ($n = 100$; $SE = 1/\sqrt{97} \approx 0.102$).

For length validation, specimens were re-imaged under a Zeiss Axio

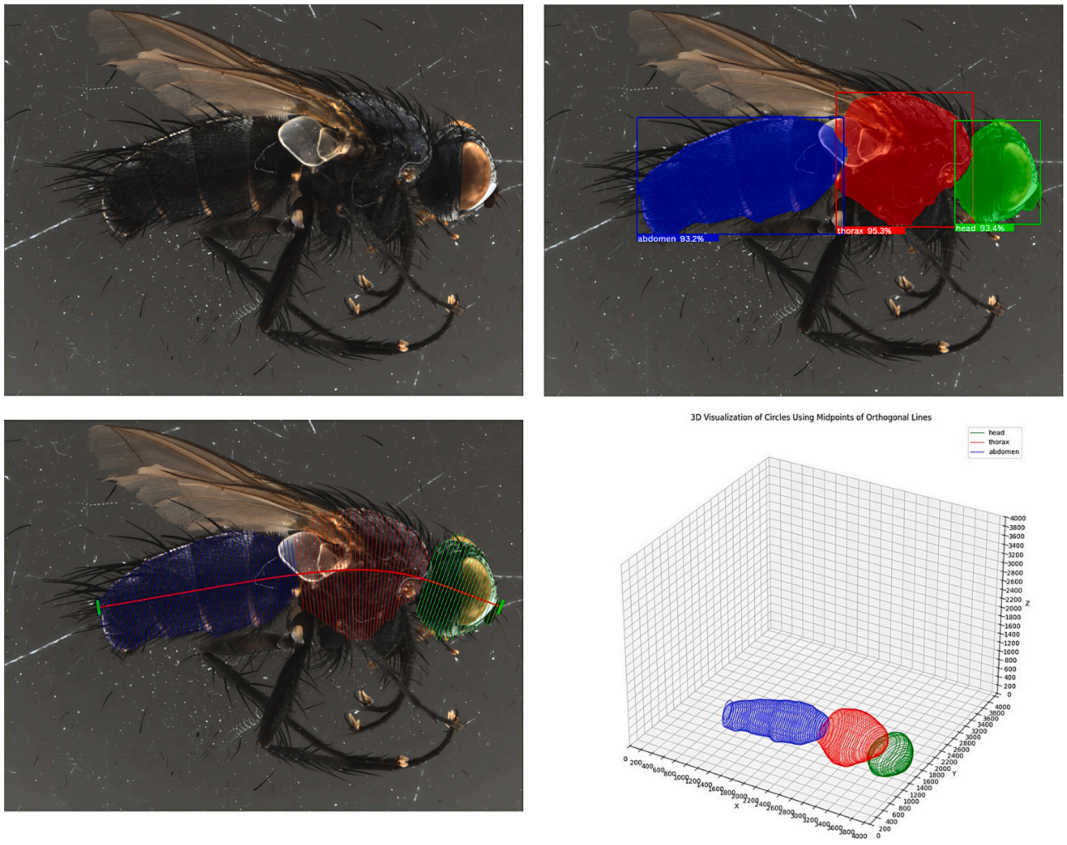

Fig. 3. Workflow for segmentation-based length and volume estimation. The input image shows an ethanol-preserved Tachinidae specimen imaged individually with the Entomoscope system. Top left: input image. Top right: predicted head, thorax, and abdomen masks. Bottom left: computationally derived centerline and orthogonal cross-sections. Bottom right: volumetric approximation generated within InsectMorphoAI using the stacked-frustum algorithm and setup-specific pixel-to-millimeter calibration; no external 3D reconstruction software was used.

Zoom V16 photomicroscope using consistent positioning. Ground truth linear length (to evaluate the OBB module) and curvilinear length (to evaluate the segmentation module) were manually measured by a single observer using Zeiss software.

To validate segmentation-derived volume as a reliable proxy for body-only biomass, wet and dry weights were obtained for all 100 specimens after leg removal. Before weighing, legs were removed to ensure consistency with the volume estimates, which are geometrically derived from the head, thorax, and abdomen masks only and thus exclude appendage mass. Therefore, the biomass validation performed here should be interpreted as validation of body-only biomass, not total organism biomass. A physical sub-analysis confirmed that dried legs constitute a substantial fraction of total dry weight (mean: 16.99% ± 4.12%; Supplementary Data S3), further justifying their removal to ensure a like-for-like comparison between geometric volume and body-only weight. For ecological applications requiring total organism biomass, the body-only estimate can therefore be interpreted either as a standardized core-body biomass proxy or adjusted using taxon-specific appendage correction factors. Replicate measurements ($n = 3$) were performed on a subset of specimens for both wet and dry weighing to ensure consistency. Specimens were weighed using a Gibertini Europe 60 scale (accuracy: 0.0001 g) for wet weights and a Gibertini E50S/3 Semi-Micro Scale (accuracy: 0.00001 g) after 24 h of desiccation at 60 °C, with weighing conducted immediately upon removal to minimize environmental rehydration.

3. Results

3.1. Performance of automated length estimation

Both computational modules accurately estimated insect length compared to manual Zeiss photomicroscope measurements across the 100 validation specimens (Table 1).

The OBB-based "Rapid Scan" module provided highly precise linear length estimates, demonstrating a strong positive linear correlation with manual measurements ($R = 0.988$, $R^2 = 0.976$), a MAE of 0.211 mm, and a RMSE of 0.290 mm. To provide ecological context, this MAE represents an error of approximately 2.26% relative to the mean specimen length in the validation set.

Similarly, the "Detailed Analysis" module successfully extracted curvilinear body length via spline interpolation, yielding strong agreement with manual curvilinear measurements ($R = 0.976$, $R^2 = 0.953$), a MAE of 0.309 mm (approximately 3.30% of mean specimen length), and a RMSE of 0.408 mm.

3.2. Body-only biomass prediction: Length vs. geometric volume

To evaluate the ecological utility of the extracted metrics, we assessed both automated length measurements and computationally derived 3D frustum volume as linear predictors of body-only biomass. As described in Section 2.5, all wet and dry weight measurements were obtained after leg removal to match the head–thorax–abdomen volume estimated by the segmentation module. We use body-only dry weight (BODW) specifically for the appendage-excluded dry-weight measurements and distinguish it from whole-specimen dry weight. Liquid displacement (Ciborowski, 1983) was evaluated as a direct volumetric reference; however, given the small specimen scale (mean BODW: 6.1 mg), measurement precision was insufficient for reliable validation; wet and dry weighing were therefore used as empirical biomass targets for validation.

Table 1
Comparison of automated length estimation accuracy against Zeiss manual ground-truth measurements.

Feature / Method	Comparison Target	Pearson R [95% CI]	R^2	MAE (mm)	RMSE (mm)
OBB linear length	Zeiss linear length	0.988 0.982–0.992	0.976	0.211	0.290
Seg. curvilinear length	Zeiss curvilinear length	0.976 0.964–0.984	0.953	0.309	0.408

While automated OBB linear length measurements showed moderate positive correlations with body-only weight (wet weight after leg removal: $R = 0.793$, $R^2 = 0.629$; BODW: $R = 0.781$, $R^2 = 0.610$), and segmentation curvilinear length performed similarly (wet weight after leg removal: $R = 0.811$, $R^2 = 0.658$; BODW: $R = 0.792$, $R^2 = 0.627$), the 3D frustum volume approximation explained more variation across both weight targets (wet weight after leg removal: $R = 0.938$ [95% CI: 0.909–0.958], $R^2 = 0.880$; BODW: $R = 0.907$ [95% CI: 0.865–0.937], $R^2 = 0.823$), as shown in Fig. 4.

Unlike length-based allometry, where power-law models are required because mass scales as the cube of linear dimensions, volume-based regression has direct physical justification: mass is proportional to density × volume, and tissue density is approximately constant within a taxon. The fitted linear regression equations for the volume-based biomass estimates are:

$$W_{wet} = 0.0314 \cdot V - 0.0135$$

$$W_{dry} = 0.0050 \cdot V - 0.0018$$

where V is the frustum-derived volume (mm^3), and W is the predicted body-only weight (g). These equations should only be applied within the volume range of the validation dataset (≥ 0.4 mm^3), as extrapolation beyond the observed range is not statistically justified for any empirical regression model. These equations are implemented in InsectMorphoAI as the default biomass conversion for Tachinidae and serve as a calibration template for users extending the pipeline to other taxa. For BODW, volume yielded $R = 0.907$ ($R^2 = 0.823$), with a MAE of 0.0010 g and a RMSE of 0.0015 g. These results demonstrate that the geometrically derived volume explained over 82% of the variance in BODW across the validation set, as visually confirmed by the tighter regression fit in panels (c) and (f) of Fig. 4.

4. Discussion

Our results illustrate how separating generalizable and taxon-specific components within a single framework can reconcile scalability with morphometric precision in automated insect morphometrics. While many insect monitoring programs primarily rely on species identification and abundance metrics, extracting standardized morphological trait data remains a bottleneck for trait-based, biomass-oriented approaches. The results presented here demonstrate that InsectMorphoAI successfully automates specimen-level morphometric data acquisition, converting standard 2D specimen images into reproducible, biologically meaningful metrics. Within the Tachinidae validation dataset, geometrically derived 3D frustum volume ($R^2 = 0.823$ for BODW; $R^2 = 0.880$ for wet weight after leg removal) explained more variation in body-only biomass than both OBB linear length ($R^2 = 0.610$ for BODW) and segmentation curvilinear length ($R^2 = 0.627$ for BODW) estimates. Importantly, this result is demonstrated within a single-family validation framework and should not be interpreted as evidence of cross-taxon generality. This supports its use as a non-destructive body-only biomass proxy within the validated taxonomic scope, while preserving specimens for downstream analyses. Furthermore, automated morphometrics eliminates the observer-dependent component of traditional protocols, ensuring fully reproducible measurements across laboratories and operators (Rogers et al., 1977; Sample et al., 1993).

4.1. Geometric precision and modular generalizability

A key finding of this study is that, within the Tachinidae validation

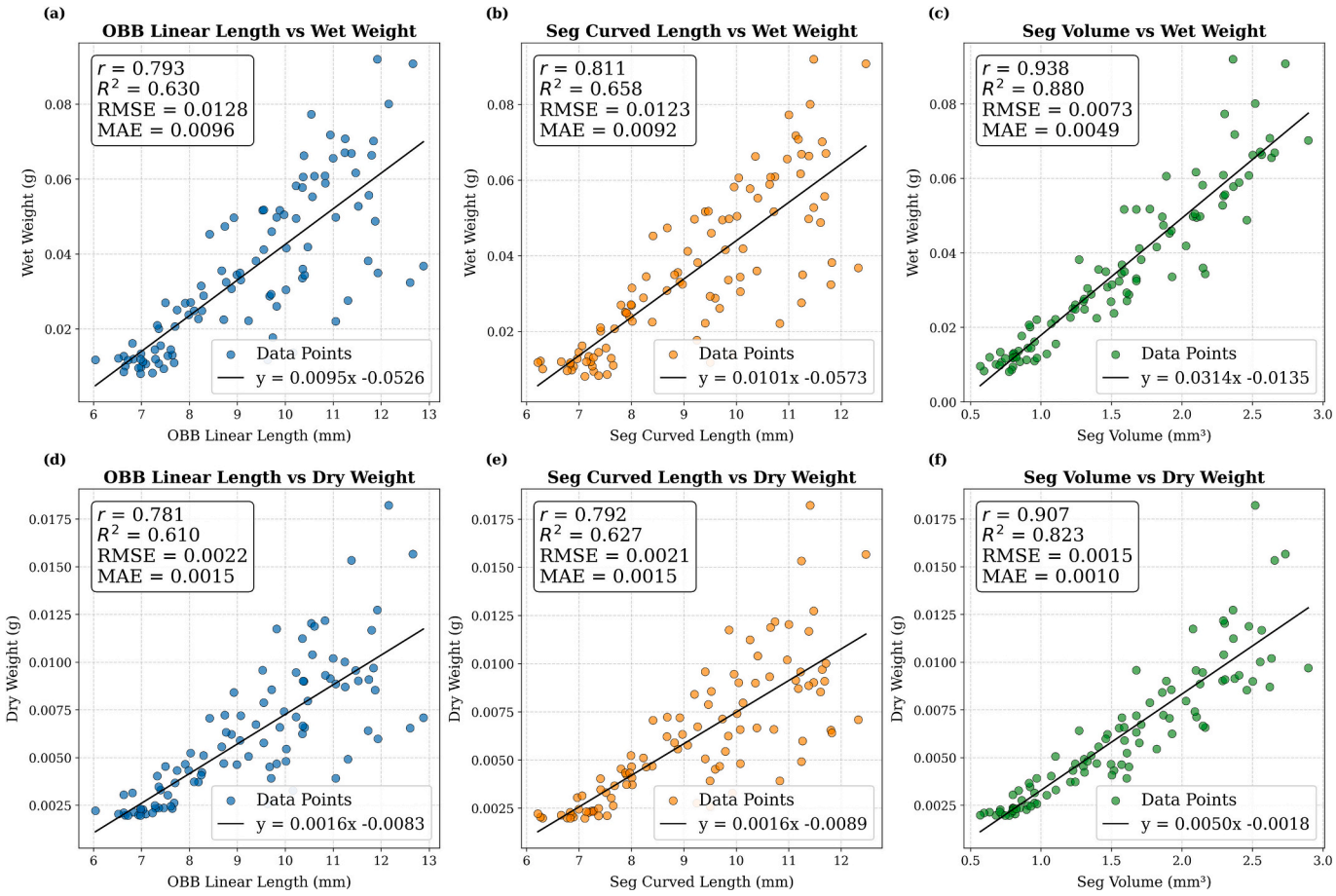

Fig. 4. Linear relationships between three image-derived features (OBB linear length, segmentation curvilinear length, and segmentation volume) and measured wet weight after leg removal (panels a–c) and body-only dry weight (BODW; panels d–f) for 100 Tachinidae specimens. Each panel displays data points, the linear regression fit (black line), and key metrics (R, R^2, MAE, RMSE).

dataset, stacked frustum volume provided a stronger body-only biomass proxy than linear or curvilinear length, while requiring only a simple linear calibration model. This parsimony is ecologically advantageous: interpretable linear models are less prone to overfitting on limited datasets and are straightforward for biologists to calibrate, communicate, and adapt to additional taxa. The strong performance of this geometric proxy suggests that, for morphometrically consistent taxa, biologically informed geometric descriptors can provide an interpretable alternative to more complex feature-engineering or black-box biomass-prediction approaches. Thus, the central contribution of the detailed-analysis module is not only the segmentation model itself, but the conversion of biologically meaningful body-part masks into an interpretable geometric volume proxy for biomass estimation.

A persistent challenge in applied computer vision for ecology is the trade-off between algorithmic generalizability and measurement precision: a model trained to precisely segment the body parts of a fly will inevitably fail when applied to a morphologically divergent taxon such as a beetle or a stick insect. InsectMorphoAI circumvents this “universal model” trap via its dual-module architecture. The OBB-based Rapid Scan module serves as a broadly applicable baseline for ecological applications — including initial size sorting of Malaise trap samples, tracking community-level shifts in body size structure over time, and providing rapid size proxies for large-scale biodiversity surveys. Because it was trained on a deliberately diverse multi-order dataset, the OBB module is expected to be more broadly applicable than the taxon-specific segmentation module and shows visually consistent predictions across representative insect groups (Fig. A3). However, formal quantitative cross-order benchmarking remains necessary to define its full taxonomic scope. Importantly, even this OBB-derived linear length proxy retains the non-destructive advantage of the framework while providing a practical size estimate for diverse bulk samples where taxon-specific segmentation training data is unavailable.

Conversely, the Detailed Analysis segmentation module acknowledges that high-precision volumetrics require taxon-specific knowledge and is particularly valuable for research questions where simple linear geometry is insufficient. Precise body-part volume estimates are directly relevant to detailed functional trait ecology (e.g., linking body composition to metabolic rates), the study of intraspecific variation such as sexual dimorphism or ontogenetic change, and the assessment of population-level responses in specific pest or beneficial species. Beyond entomological monitoring, pollination research could benefit from automated morphometric extraction because body-size-related traits are often relevant to foraging range, pollen transport capacity, and plant–pollinator trait matching. However, pollination efficiency should not be inferred from body size alone, as it also depends on flower visitation rate, seasonal phenology, daily activity patterns, pollen-placement mechanisms, foraging preferences, and sociality. For bee-focused applications, future extensions of InsectMorphoAI could also target intertegular distance or other taxon-specific landmark measurements (Greenleaf et al., 2007), which may be more appropriate than body length for some pollination-related questions. By deploying this module as an extensible framework and providing our iterative pseudo-label refinement pipeline as an open-source blueprint, researchers can train highly precise models tailored to their specific focal taxa. Importantly, however, each additional family will require dedicated annotation, performance evaluation, and biomass calibration before high-

precision volumetric estimates can be interpreted ecologically. Given that rank-abundance distributions in Malaise trap samples are typically dominated by a limited number of families (Srivathsan et al., 2023), developing specialized segmentation models for the most frequent families remains a tractable and high-impact extension. Beyond whole-body morphometrics, the same modular training pipeline could be extended to extract ecologically relevant sub-features, such as proboscis length in pollinators.

4.2. Comparative analysis with existing frameworks

While several automated morphometric pipelines have been introduced in recent years, they occupy distinct operational niches. InsectMorphoAI is designed to fill a specific gap: providing accessible, hardware-agnostic, granular trait extraction for standard biological laboratories. A comparison of core features between InsectMorphoAI and existing state-of-the-art tools is provided in Table 2.

As outlined in Table 2, tools like DiversityScanner offer high physical throughput via robotic automation, but this comes at the cost of accessibility for standard laboratories. Notably, whereas DiversityScanner estimates length by summing straight-line segments across individual body parts, InsectMorphoAI fits a continuous parametric cubic spline through the body axis, yielding a true curvilinear measurement that more accurately captures specimens fixed in curved postures. Similarly, BIODISCOVER (Ärje et al., 2020) relies on a custom robotic imaging platform, and specimens must be fed manually without post-processing sorting, limiting its throughput and accessibility. At the other end of the spectrum, Schneider et al. (2022) maximize throughput by estimating functional-group-level biomass from bulk sample images, but a 2D pixel area is an inherently inconsistent predictor of volume across taxa with complex shapes or varying depth profiles. InsectMorphoAI occupies the intermediate niche: frustum-based geometric precision at the individual specimen level, deployable in any standard laboratory without dedicated hardware. In practical ecological workflows, InsectMorphoAI can serve as a morphometric layer between specimen digitization and downstream ecological analysis. After individual specimens are imaged, the OBB module can rapidly generate standardized length estimates for large sample sets, supporting size-structure analyses, specimen sorting, and community-level comparisons across sites or time points. For focal taxa for which segmentation models have been trained and validated, the Detailed Analysis module can provide higher-resolution body-part measurements, curvilinear length, and body-only biomass estimates. These outputs can be exported as analysis-ready CSV files and linked to taxonomic identifications, DNA barcodes, sampling metadata, or environmental variables. Compared with manual measurement and weighing, this workflow is non-destructive, reproducible, less observer-dependent, and better suited to high-throughput monitoring pipelines in which specimens must remain available for downstream molecular or taxonomic analyses.

4.3. Limitations and future directions

First, as detailed in Section 2.4.3, the stacked-frustum calculation assumes that each 2D mask-derived body width approximates the diameter of a circular cross-section. This assumption is biologically plausible for the relatively cylindrical body plan of Tachinidae, which is why this family was suitable for the present proof-of-concept validation, but deviations from this geometry will directly affect volume and biomass estimates. For dorsoventrally flattened taxa, the method may overestimate volume because body depth is smaller than the visible dorsal width; for laterally compressed or irregularly shaped taxa, the direction and magnitude of bias may be less predictable. Similarly, dense setation, folded wings, damaged specimens, and appendages obscuring body boundaries may distort the estimated cross-sectional diameters. These limitations do not invalidate the method for Tachinidae, but they define the current boundaries of applicability. Future versions could incorporate elliptical or taxon-specific cross-sectional models, multi-view imaging, or calibration factors derived from physical measurements to reduce such biases.

Second, the volume estimation is derived solely from the head, thorax, and abdomen masks to avoid severe pixel noise introduced by highly articulated legs, wings, and antennae. Consequently, the biomass equations validated here estimate body-only biomass rather than total organism biomass. This distinction is important because ecological applications differ in whether they require standardized core-body biomass or whole-specimen biomass. In our Tachinidae validation set, dried legs represented 16.99% ± 4.12% of total dry weight, showing that appendages can contribute a non-negligible fraction of total mass. For applications requiring total organism biomass, future implementations could incorporate taxon-specific correction factors, appendage segmentation models, or separate calibration equations based on whole-specimen weights. Until such calibration is available, the current equations should be interpreted as body-only biomass estimates. Additionally, while the annotation strategy was designed to handle partial occlusions, near-complete concealment of a body segment by folded wings or overlapping legs remains a boundary case that may reduce segmentation reliability; visual inspection of outputs is advisable in such instances.

Third, the current models were trained on ethanol-preserved, individually imaged specimens acquired under controlled conditions using the Entomoscope setup. Performance on less standardized biodiversity-monitoring images, including field-taken images, mixed bulk-sample images, overlapping individuals, damaged specimens, or specimens prepared by alternative methods such as dry-pinned, point-mounted, or critical-point-dried material, has not been formally evaluated. Future work should assess these conditions through formal domain-shift

Table 2
Feature comparison of state-of-the-art automated insect morphometric software.

Feature	InsectMorphoAI (this study)	DiversityScanner (Wührl et al., 2022)	BIODISCOVER (Ärje et al., 2020)	Schneider et al. (2022)
Primary morphometric proxy	OBB linear length & segmentation curvilinear length; 3D frustum volume	Linear length & 3D body volume (orthogonal cross-section slices)	2D geometric image features	2D pixel area × group-specific density
Measurement granularity	Specimen-level, per body part	Specimen-level	Specimen-level	Functional-group level
Hardware dependency	Hardware-agnostic (any camera or microscope)	Requires an integrated custom robotic imaging platform	Requires a custom robotic BIODISCOVER imaging machine	Hardware-agnostic (standard camera)
Specimen size range	Flexible; depends on imaging setup and calibration	Optimized for specimens <3 mm	Not specified	Not specified
Set up and accessibility	Docker container with Streamlit GUI; Python CLI	Integrated robotic platform (hardware + embedded software)	Custom robotic BIODISCOVER platform	Standard camera + Python
Non-destructive	Yes	Yes	Yes	Yes
Ideal use case	Accessible specimen-level morphometrics for any lab	High-throughput robotic digitization of small (<3 mm) insects at specialized facilities	Automated specimen identification with hardware-based imaging	Functional-group classification and biomass from bulk sample photos

benchmarking across taxa, specimen preparations, and imaging platforms. Such validation could also quantify robustness under controlled perturbations and incorporate confidence-based quality flags to identify cases requiring manual inspection. Future benchmarking could also evaluate newer object-detection and instance-segmentation architectures to determine whether alternative spatial modeling strategies improve body-part segmentation for highly articulated or strongly contorted insect specimens.

Beyond these current constraints, several directions offer promising avenues for future development. A particularly tractable extension is the application of the volume estimation pipeline to larval stages, which are particularly challenging for traditional approaches due to their small size and rapid desiccation post-collection. Photographing live larvae, temporarily immobilized via brief cold exposure, could enable non-destructive volume tracking across molting events, offering a new tool for developmental ecology and growth rate studies.

While the OBB module was trained on a multi-order dataset spanning Diptera, Hymenoptera, and Coleoptera, and its generalizability is qualitatively demonstrated in Fig. A3, formal cross-order benchmarking with quantitative error metrics remains a natural next step to characterize its taxonomic scope further. Future software extensions could also target bulk-sample imaging, where multiple specimens appear within a single frame; in such scenarios, the segmentation pipeline would require integration of robust instance separation logic to prevent merged masks from adjacent individuals.

5. Conclusion

InsectMorphoAI provides a validated, open-source, and hardware-agnostic framework for automated insect morphometrics from standard 2D images. The dual-module architecture combines a broadly applicable OBB-based length estimator with a taxon-specific instance segmentation pipeline that currently provides validated high-precision volumetric extraction for Tachinidae. A key finding is that, within the Tachinidae validation dataset, geometrically derived 3D frustum volume ($R^2 = 0.823$ for body-only dry weight) yielded higher explanatory power for body-only dry weight than linear length ($R^2 = 0.610$), while requiring only a simple linear calibration model. This makes the approach interpretable and provides a calibration template for future taxon-specific extensions. Being fully non-destructive, the framework integrates naturally into modern reverse-workflow biodiversity pipelines by allowing specimens to be imaged, morphometrically quantified, exported as structured trait data, and then retained for downstream taxonomic or molecular analyses such as DNA barcoding. The current limitations, including taxon-specific segmentation, circular cross-section assumptions, and training on ethanol-preserved material, define the present boundaries of applicability. Addressing these limitations through additional taxon-specific datasets, alternative geometric models, and cross-condition validation would substantially extend the software's ecological reach. By making specimen-level morphometric precision accessible to any standard laboratory, InsectMorphoAI addresses a key bottleneck in trait-based and biomass-oriented high-throughput biodiversity monitoring.

Declaration of generative AI and AI-assisted technologies in the manuscript preparation process.

During the preparation of this work, the authors used AI tools to improve clarity and fluency in their writing. After using these tools, the authors reviewed and edited the content as needed and take full responsibility for the content of the published article.

CRediT authorship contribution statement

Hossein Shirali: Writing – review & editing, Writing – original draft, Visualization, Software, Methodology, Investigation, Formal analysis, Data curation, Conceptualization. **Aleida Ascenzi:** Writing – review & editing, Writing – original draft, Validation, Resources, Investigation, Formal analysis, Data curation, Conceptualization. **Lorenz Wührl:** Writing – review & editing, Methodology, Conceptualization. **Nils Beyer:** Validation, Software. **Noemi Di Lorenzo:** Validation, Resources, Data curation. **Emanuele Vaccarella:** Validation, Resources. **Nathalie Klug:** Writing – review & editing, Methodology. **Rudolf Meier:** Writing – review & editing, Supervision, Project administration, Funding acquisition. **Pierfilippo Cerretti:** Writing – review & editing, Supervision, Project administration, Funding acquisition, Conceptualization. **Christian Pylatiuk:** Writing – original draft, Supervision, Project administration, Funding acquisition, Conceptualization.

Funding

Our work was supported by funding from: the Center for Integrative Biodiversity Discovery at the Museum für Naturkunde Berlin and by grant #ZF4717901SK9 of the program Natural, Artificial and Cognitive Information Processing (NACIP) of the Helmholtz-Association, Germany; Helmholtz Association Initiative and Networking Fund on the HAICORE@KIT partition; European Union–NextGenerationEU as part of the National Biodiversity Future Center, Italian National Recovery and Resilience Plan (NRRP) Mission 4 Component 2 Investment 1.4 (CUP: B83C22002950007).

Declaration of competing interest

The authors declare no conflicts of interest.

Appendix A. Supplementary data

Supplementary data to this article can be found online at https://doi.org/10.1016/j.ecoinf.2026.103854.

Data availability

Image datasets and validation data are available on Zenodo; InsectMorphoAI source code, installation instructions, and demo video are available on GitLab.

References

Ärje, J., Melvad, C., Jeppesen, M.R., Madsen, S.A., Raitoharju, J., Rasmussen, M.S., Iosifidis, A., Tirronen, V., Gabbouj, M., Meissner, K., Høye, T.T., 2020. Automatic image-based identification and biomass estimation of invertebrates. Methods in Ecology and Evolution 11 (8), 922–931. https://doi.org/10.1111/2041-210X.13428.

Ascenzi, A., Wührl, L., Feng, V., Klug, N., Pylatiuk, C., Cerretti, P., Meier, R., 2025. EntoSieve: automated size-sorting of insect bulk samples to aid accurate megabarcoding and metabarcoding. Mol. Ecol. Resour., e14097 https://doi.org/10.1111/1755-0998.14097.

Bartomeus, I., Gravel, D., Tylianakis, J.M., Aizen, M.A., Dickie, I.A., Bernard-Verdier, M., 2016. A common framework for identifying linkage rules across different types of interactions. Funct. Ecol. 30 (12), 1894–1903. https://doi.org/10.1111/1365-2435.12666.

Bosch, J., Vicens, N., 2002. Body size as an estimator of production costs in a solitary bee. Ecological Entomology 27 (2), 129–137. https://doi.org/10.1046/j.1365-2311.2002.00406.x.

Cardinale, B.J., Duffy, J.E., Gonzalez, A., Hooper, D.U., Perrings, C., Venail, P., Narwani, A., Mace, G.M., Tilman, D., Wardle, D.A., Kinzig, A.P., Daily, G.C., Loreau, M., Grace, J.B., Larigauderie, A., Srivastava, D.S., Naeem, S., 2012. Biodiversity loss and its impact on humanity. Nature 486 (7401), 59–67. https://doi.org/10.1038/nature11148.

Caruso, V., Shirali, H., Bouget, C., Cerretti, P., Curletti, G., de Groot, M., Groznik, E., Gutowski, J.M., Pylatiuk, C., Plewa, R., Roques, A., Sallé, A., Sweeney, J., Van Rooyen, K., Wührl, L., Rassati, D., 2026. Image-based recognition using advanced neural networks can aid surveillance of Agrilus jewel beetles. NeoBiota 105, 319–336. https://doi.org/10.3897/neobiota.105.180959.

Ciborowski, J.J.H., 1983. A simple volumetric instrument to estimate biomass of fluid-preserved invertebrates. The Canadian Entomologist 115 (4), 427–430. https://doi.org/10.4039/Ent115427-4.

Ganihar, S.R., 1997. Biomass estimates of terrestrial arthropods based on body length. J. Biosci. 22 (2), 219–224. https://doi.org/10.1007/BF02704734.

Greenleaf, S.S., Williams, N.M., Winfree, R., Kremen, C., 2007. Bee foraging ranges and their relationship to body size. Oecologia 153, 589–596. https://doi.org/10.1007/s00442-007-0752-9.

Hallmann, C.A., Sorg, M., Jongejans, E., Siepel, H., Hofland, N., Schwan, H., Stenmans, W., Müller, A., Sumser, H., Hörren, T., Goulson, D., de Kroon, H., 2017. More than 75 percent decline over 27 years in total flying insect biomass in protected areas. PloS One 12 (10), e0185809. https://doi.org/10.1371/journal.pone.0185809.

Hartop, E., Srivathsan, A., Ronquist, F., Meier, R., 2022. Towards large-scale integrative taxonomy (LIT): resolving the data conundrum for dark taxa. Syst. Biol. 71 (6), 1404–1422. https://doi.org/10.1093/sysbio/syac033.

Hartop, E., Lee, L., Srivathsan, A., Jones, M., Peña-Aguilera, P., Ovaskainen, O., Roslin, T., Meier, R., 2024. Resolving biology's dark matter: species richness, spatiotemporal distribution, and community composition of a dark taxon. BMC Biol. 22 (1), 215. https://doi.org/10.1186/s12915-024-02010-z.

He, K., Gkioxari, G., Dollár, P., Girshick, R., 2017. Mask R-CNN, in: Proceedings of the IEEE International Conference on Computer Vision (ICCV). IEEE, Venice, pp. 2961–2969. https://doi.org/10.1109/ICCV.2017.322.

Helicon Soft Ltd., 2025. Helicon Focus (Version 8) [WWW Document]. URL https://www.heliconsoft.com/heliconsoft-products/helicon-focus/ (accessed 12 May 2025).

Hereld, M., Ferrier, N.J., Agarwal, N., Sierwald, P., 2017. Designing a high-throughput pipeline for digitizing pinned insects. In: 2017 IEEE 13th international conference on E-science (e-science). IEEE, pp. 542–550. https://doi.org/10.1109/eScience.2017.88.

Jocher, G., Chaurasia, A., Qiu, J., 2023. Ultralytics YOLO (version 8.0.0) [software]. URL. https://github.com/ultralytics/ultralytics.

Karlsson, D., Forshage, M., Holston, K., Ronquist, F., 2020. The data of the Swedish malaise trap project, a countrywide inventory of Sweden's insect fauna. Biodiversity Data Journal 8, e56286. https://doi.org/10.3897/BDJ.8.e56286.

Kirillov, A., Mintun, E., Ravi, N., Mao, H., Rolland, C., Gustafson, L., Xiao, T., Whitehead, S., Berg, A.C., Lo, W.-Y., Dollár, P., Girshick, R., 2023. Segment anything (no. arXiv:2304.02643). arXiv. https://doi.org/10.48550/arXiv.2304.02643.

Klug, N., Kramer, M., Mazrek, F., Wührl, L., Shirali, H., Meier, R., Pylatiuk, C., 2024. Automated photogrammetric close-range imaging system for small invertebrates using acoustic levitation. TechRxiv. https://doi.org/10.36227/techrxiv.172651022.21831566/v1.

Knyshov, A., Hoang, S., Weirauch, C., 2021. Pretrained convolutional neural networks perform well in a challenging test case: identification of plant bugs (Hemiptera: Miridae) using a small number of training images. Insect Systematics and Diversity 5 (2), 3. https://doi.org/10.1093/isd/ixab004.

LaBarbera, M., 1989. Analyzing body size as a factor in ecology and evolution. Annu. Rev. Ecol. Evol. Syst. 20, 97–117. https://doi.org/10.1146/annurev.es.20.110189.000525.

Lister, B.C., Garcia, A., 2018. Climate-driven declines in arthropod abundance restructure a rainforest food web. Proc. Natl. Acad. Sci. 115 (44), E10397–E10406. https://doi.org/10.1073/pnas.1722477115.

Liu, S., Zeng, Z., Ren, T., Li, F., Zhang, H., Yang, J., Li, C., Yang, J., Su, H., Zhu, J., Zhang, L., 2023. Grounding DINO: marrying DINO with grounded pre-training for open-set object detection (no. arXiv:2303.05499). arXiv. https://doi.org/10.48550/arXiv.2303.05499.

Loreau, M., Naeem, S., Inchausti, P., Bengtsson, J., Grime, J.P., Hector, A., Hooper, D.U., Huston, M.A., Raffaelli, D., Schmid, B., Tilman, D., Wardle, D.A., 2001. Biodiversity and ecosystem functioning: current knowledge and future challenges. Science 294 (5543), 804–808. https://doi.org/10.1126/science.1064088.

Maurey, E., Marrec, R., Brusse, T., Le Provost, G., Le Roux, V., Bergerot, B., Caro, G., 2025. When size matters: a morphological measurement that informs on the potential pest control function by soil arthropod communities. J. Pest. Sci. https://doi.org/10.1007/s10340-025-01879-1.

Meier, R., Hartop, E., Pylatiuk, C., Srivathsan, A., 2024. Towards holistic insect monitoring: species discovery, description, identification and traits for all insects. Philos. Trans. R. Soc., B 379 (1904), 20230120. https://doi.org/10.1098/rstb.2023.0120.

O'Hara, J.E., Henderson, S.J., 2022. Cataloguing the world Tachinidae (Diptera). The Tachinid Times 35, 4–21.

Ramalho, M., Imperatriz-Fonseca, V.L., Giannini, T.C., 1998. Within-colony size variation of foragers and pollen load capacity in the stingless bee Melipona quadrifasciata anthidioides Lepeletier (Apidae, Hymenoptera). Apidologie 29 (3), 221–228. https://doi.org/10.1051/apido:19980302.

Rogers, L.E., Hinds, W.T., Buschbom, R.L., 1977. A general weight vs. length relationship for insects. Ann. Entomol. Soc. Am. 69 (2), 387–389. https://doi.org/10.1093/aesa/69.2.387.

Sample, B.E., Cooper, R.J., Greer, R.D., Whitmore, R.C., 1993. Estimation of insect biomass by length and width. Am. Midl. Nat. 129 (2), 234–240. https://doi.org/10.2307/2426503.

Sánchez-Bayo, F., Wyckhuys, K.A.G., 2019. Worldwide decline of the entomofauna: a review of its drivers. Biol. Conserv. 232, 8–27. https://doi.org/10.1016/j.biocon.2019.01.020.

Schneider, S., Taylor, G.W., Kremer, S.C., Burgess, P., McGroarty, J., Mitsui, K., Zhuang, A., deWaard, J.R., Fryxell, J.M., 2022. Bulk arthropod abundance, biomass and diversity estimation using deep learning for computer vision. Methods Ecol. Evol. 13 (2), 346–357. https://doi.org/10.1111/2041-210X.13769.

Shirali, H., Ascenzi, A., 2026. Annotated insect image dataset for InsectMorphoAI [data set]. Zenodo. https://doi.org/10.5281/zenodo.18959238.

Shirali, H., Hübner, J., Both, R., Raupach, M., Reischl, M., Schmidt, S., Pylatiuk, C., 2024. Image-based recognition of parasitoid wasps using advanced neural networks. Invertebr. Syst. 38 (6). https://doi.org/10.1071/IS24011.

Shirali, H., Ascenzi, A., Wührl, L., Beyer, N., Di Lorenzo, N., Vaccarella, E., Klug, N., Meier, R., Cerretti, P., Pylatiuk, C., 2026b. InsectMorphoAI. GitLab. https://gitlab.kit.edu/kit/iai/ber/insectmorphoAI.

Shirali, H., Wührl, L., Lee, L., Klug, N., Meier, R., Pylatiuk, C., Hartop, E., 2026c. Automated specimen triage for dark taxa: deep learning enables orientation, sex identification and anatomical segmentation from robotic imaging. Syst. Entomol. https://doi.org/10.1111/syen.70039.

Smock, L.A., 1980. Relationships between body size and biomass of aquatic insects. Freshw. Biol. 10 (4), 375–383. https://doi.org/10.1111/j.1365-2427.1980.tb01211.x.

Srivathsan, A., Lee, L., Katoh, K., Hartop, E., Kutty, S.N., Wong, J., Yeo, D., Meier, R., 2021. ONTbarcoder and MinION barcodes aid biodiversity discovery and identification by everyone, for everyone. BMC Biol. 19 (1), 217. https://doi.org/10.1186/s12915-021-01141-x.

Srivathsan, A., Ang, Y., Heraty, J.M., Hwang, W.S., Jusoh, W.F.A., Kutty, S.N., Puniamoorthy, J., Yeo, D., Roslin, T., Meier, R., 2023. Convergence of dominance and neglect in flying insect diversity. Nature Ecology & Evolution 7 (7), 1143–1151. https://doi.org/10.1038/s41559-023-02066-0.

Stireman III, J.O., Cerretti, P., O'Hara, J.E., Moulton, J.K., 2021. Extraordinary diversification of the "bristle flies" (Diptera: Tachinidae) and its underlying causes. Biol. J. Linn. Soc. 133 (1), 216–236. https://doi.org/10.1093/biolinnean/blab010.

Streamlit Inc., n.d. Streamlit: A Faster Way to Build and Share Data Apps [WWW Document]. URL https://streamlit.io/ (accessed 10 March 2026).

Streinzer, M., Huber, W., Spaethe, J., 2016. Body size limits dim-light foraging activity in stingless bees (Apidae: Meliponini). J. Comp. Physiol. A 202, 643–655. https://doi.org/10.1007/s00359-016-1118-8.

Van Dam, A.R., Štarhová Serbina, L., 2025. Descriptron: artificial intelligence for automating taxonomic species descriptions with a user-friendly software package. Syst. Entomol. 51 (1), e70005. https://doi.org/10.1111/syen.70005.

Wada, K., 2018. Labelme: image polygonal annotation with Python. Zenodo. https://doi.org/10.5281/zenodo.5711226.

Wägele, J.W., Bodesheim, P., Bourlat, S.J., Denzler, J., Diepenbroek, M., Fonseca, V., Frommolt, K.-H., Geiger, M.F., Gemeinholzer, B., Glöckner, F.O., Haucke, T., Kirse, A., Kölpin, A., Kostadinov, I., Kühl, H.S., Kurth, F., Lasseck, M., Liedke, S., Losch, F., Müller, S., Petrovskaya, N., Piotrowski, K., Radig, B., Scherber, C., Schoppmann, L., Schulz, J., Steinhage, V., Tschan, G.F., Vautz, W., Velotto, D., Weigend, M., Wildermann, S., 2022. Towards a multisensor station for automated biodiversity monitoring. Basic Appl. Ecol. 59, 105–138. https://doi.org/10.1016/j.baae.2022.01.003.

Wührl, L., Pylatiuk, C., Giersch, M., Lapp, F., von Rintelen, T., Balke, M., Schmidt, S., Cerretti, P., Meier, R., 2022. DiversityScanner: robotic handling of small invertebrates with machine learning methods. Mol. Ecol. Resour. 22 (4), 1626–1638. https://doi.org/10.1111/1755-0998.13567.

Wührl, L., Rettenberger, L., Meier, R., Hartop, E., Graf, J., Pylatiuk, C., 2024. Entomoscope: an open-source photomicroscope for biodiversity discovery. IEEE Access 12, 11785–11794. https://doi.org/10.1109/ACCESS.2024.3355272.

Xia, G.-S., Bai, X., Ding, J., Zhu, Z., Belongie, S., Luo, J., Datcu, M., Pelillo, M., Zhang, L., 2018. DOTA: A Large-Scale Dataset for Object Detection in Aerial Images, in: Proceedings of the IEEE/CVF Conference on Computer Vision and Pattern Recognition (CVPR). IEEE, Salt Lake City, UT, pp. 3974–3983. https://doi.org/10.1109/CVPR.2018.00418.

Yeo, D., Srivathsan, A., Puniamoorthy, J., Maosheng, F., Grootaert, P., Chan, L., Guénard, B., Damken, C., Wahab, R.A., Yuchen, A., Meier, R., 2021. Mangroves are an overlooked hotspot of insect diversity despite low plant diversity. BMC Biol. 19 (1), 202. https://doi.org/10.1186/s12915-021-01088-z.